Refereed Proceedings

The 12th International Conference on Fluidization - New Horizons in Fluidization Engineering

Numerical Investigation of the Layer-Inversion Phenomenon in Binary Solid Liquid Fluidized Beds

Kevin F. Malone*   Bao H. Xu[†]

Michael Fairweather[‡]

*University of Leeds, chekfm@leeds.ac.uk
[†]University of Leeds, b.h.xu@leeds.ac.uk
[‡]University of Leeds

Malone et al.: Numerical Investigation of the Layer-Inversion Phenomenon

NUMERICAL INVESTIGATION OF THE LAYER-INVERSION PHENOMENON IN BINARY-SOLID LIQUID FLUIDIZED BEDS

Kevin F. Malone, Bao H. Xu, Michael Fairweather
Institute of Particle Science and Engineering
University of Leeds, Leeds LS2 9JT, UK
T: +44-113-343-2423; F: +44-113-343-2405; E: b.h.xu@leeds.ac.uk

ABSTRACT

Layer inversion behaviour in binary-solid liquid fluidized beds is examined using a Combined Continuum and Discrete Model. A suitable bidisperse system was selected from information in the literature. By simulating the fluidization of the system at a range of liquid velocities, varying degrees of segregation and mixing have been observed.

INTRODUCTION

Binary systems consisting of two distinct particulate components can often have a tendency to segregate when fluidized with a liquid, if there is a sufficient difference in particle size, density, or even shape (1) between the two component species. The extent of segregation depends on the size/density/shape difference between the two species – if this is sufficiently large the bed can form two distinct layers; alternatively, if the difference is small a mixing zone will exist between the layers.

For the special case of a binary mixture where the species differ in particle size and density such that the large particles are the less dense, the system may exhibit a very interesting phenomenon – layer-inversion. At low liquid velocities, the larger, less dense particles occupy the top of the bed and form a layer above the smaller, denser species. Increasing the liquid velocity through a critical value causes the layers to invert, i.e. the larger particles move to the lower part of the bed.

Layer-inversion was first examined experimentally by Moritomi *et al.* (2), who observed that it could be induced in two ways in suitable systems: by varying the liquid velocity, or by varying the solids composition of the bed at fixed liquid velocity. Several studies of the phenomenon have since been carried out, mostly using an experimental approach (3-11), although some purely analytical work has been presented (12, 13). Simulations using continuum models have also been reported (14, 15), but no studies using a discrete-particle approach have been presented.

A number of models for predicting the layer-inversion phenomenon have been proposed, often derived from quite different theoretical bases. Many of these models have recently been compared by Escudié *et al.* (16), who noted that there was a considerable degree of uncertainty in their comparison, as the predictions were

sensitive to the liquid viscosity, a parameter that depends strongly on temperature, which was not recorded in many of the experimental works.

In this work, we examine the layer-inversion phenomenon in liquid fluidized beds using the Combined Continuum and Discrete Model (CCDM), a computational method for simulating multiphase particle-flow systems. Simulations have the advantage of being able to easily manipulate and control system parameters such as the fluid properties and the particle sizes and densities. CCDM's ability to track individual particles makes it a powerful technique for investigating mixing and segregation in fluidized beds, since the bed composition can be calculated based on the positions of all the particles, rather than on only a small sample.

METHODOLOGY

CCDM combines the Discrete Element Method (DEM) for predicting the particle motion with Computational Fluid Dynamics (CFD) for the continuum fluid flow. In DEM ([17]) simulations, the trajectories and rotations of individual particles are evaluated based on Newton's 2nd law of motion, using a numerical time stepping scheme. Contact forces are calculated at each time step using appropriate contact laws, and resolved into their normal and tangential components. The key assumption in DEM is that disturbances cannot propagate from any particle further than its immediate neighbours, providing a sufficiently small time step is used.

For the fluid flow, the locally-averaged ([18]) continuity and Navier-Stokes equations are solved using the SIMPLE method ([19]) to give the fluid velocity and pressure. This CFD calculation is combined with the DEM simulation by carefully applying Newton's 3rd law of motion to the fluid-particle interaction force. This ensures the two sets of equations, which are solved on different length scales, are correctly coupled. Full details of the CCDM model formulation as applied in gas-fluidized beds are given in ([20]). Modifications for simulating liquid-solid systems are described below.

Fluid-particle interaction forces

In liquid systems, the low density difference between the phases means some fluid-particle interactions that are negligible in gas systems must be considered. In this work we consider added-mass, Magnus lift, and pressure gradient forces in addition to the steady state drag force. The overall fluid-particle interaction force is therefore:

$$\mathbf{f}_d = \frac{\pi}{6}\rho_f d_p{}^3 \left[\begin{array}{c} \frac{3}{4d_p}\left(C_{D0}\left|\mathbf{u}_f - \mathbf{u}_p\right|\left(\mathbf{u}_f - \mathbf{u}_p\right)\varepsilon^{-\chi+1} + C_m\left(\mathbf{u}_f - \mathbf{u_p}\right)^2\right) \\ + C_a\frac{d}{dt}\left(\mathbf{u}_f - \mathbf{u_p}\right) + \left(\frac{d\mathbf{u}_f}{dt} - \mathbf{g}\right) \end{array} \right] \qquad [1]$$

where ρ_f is the fluid density, d_p is the particle diameter, ε is the voidage, $\mathbf{g}$ is gravitational acceleration, and $\mathbf{u}_f$ and $\mathbf{u}_p$ are respectively the fluid and particle velocities. C_{D0}, the steady drag coefficient, and the exponent χ are functions of the particle Reynolds number, Re_p, as given in ([21]). C_m, the Magnus lift coefficient, is also a function of Re_p, and is calculated as described in ([22]). C_a is the added-mass coefficient, taken to be 0.5. The final term in brackets is the pressure gradient ([23]).[2]

Particle-particle and particle-wall contacts

In liquid systems, interparticle collisions differ from those in gas systems due to lubrication forces between the particle surfaces, which depend on the fluid density and viscosity. To account for this in CCDM, each particle's coefficient of restitution is taken to be a function of the particle Stokes number ([24]):

$$e_{liquid} = e_{gas}\left(1 - \frac{St_c}{St}\right)$$ [2]

where e_{gas} is the particle coefficient of restitution in air, and St_c is the critical impact Stokes number, below which rebound does not occur. In this work, St_c was set equal to 10 ([24]). St, the particle Stokes number, is given by:

$$St = \frac{4m_p u_p}{6\pi\mu d_p^{\ 2}} = \frac{Re_p}{9}\frac{\rho_p}{\rho_f}$$ [3]

where m_p is the particle's mass and μ is the fluid viscosity.

SIMULATION PARAMETERS

For this initial study it was decided to investigate a system of constant composition, where the bed contained the same volume of each species, in which inversion would be produced solely by altering the liquid velocity. Basing this system on literature data would make the DEM computation prohibitively expensive, as the large particle size differences used would require a large number of particles. For this reason, it was decided to use a water-fluidized system where the particle diameters varied by a factor of two, meaning that only eight small particles were needed for each large particle. The size and density of the larger component (A) were taken arbitrarily to be those of 5mm glass beads. The diameter of the smaller particles (B) was therefore taken to be 2.5mm. The density of B was then selected based on ([2]) as follows; the bulk density of a bed of pure species x, ρ_{bx}, is given by:

$$\rho_{bx} = \varepsilon_x \rho_f + \left(1 - \varepsilon_x\right)\rho_x$$ [4]

where ρ_x is the density of the solid. The voidage ε_x is a function of the liquid velocity, u_f, as given by the Richardson-Zaki equation ([25]):

$$\varepsilon_x^{n_x} = u_f / u_{tx}$$ [5]

where u_{tx} is the terminal velocity of a particle of x, estimated using ([26]):

$$Re_{tx} = \left(1 - 1.15\left(\frac{d}{D}\right)^{0.6}\right)\left(2.33Ga_x^{\ 0.018} - 1.53Ga_x^{\ -0.016}\right)^{13.3}$$ [6]

where Re_{tx} is the terminal particle Reynolds number, and D is the bed diameter. n_x

was determined from (26):

$$\frac{4.8-n_x}{n_x-2.4}=0.043\,\text{Ga}_x^{0.57}\left(1-1.24\left(\frac{d}{D}\right)^{0.27}\right)$$ [7]

The Galileo number, Ga_x, is defined as:

$$\text{Ga}_x=d_{px}^3\rho_f\left(\rho_x-\rho_f\right)g\big/\mu^2$$ [8]

By substituting using equation [5] for ε_x in equation [4], an expression may be obtained for the bulk density in terms of ρ_x, n_x, u_f and u_{tx}. It is thus possible to produce a plot of bulk density, ρ_x, against liquid velocity, u_f, for each component. By trial and error manipulation of the density of component B, it was possible to obtain a system where the two bulk density curves cross somewhere in the operable range (between the limits of minimum fluidization and terminal velocities), as in Figure 1.
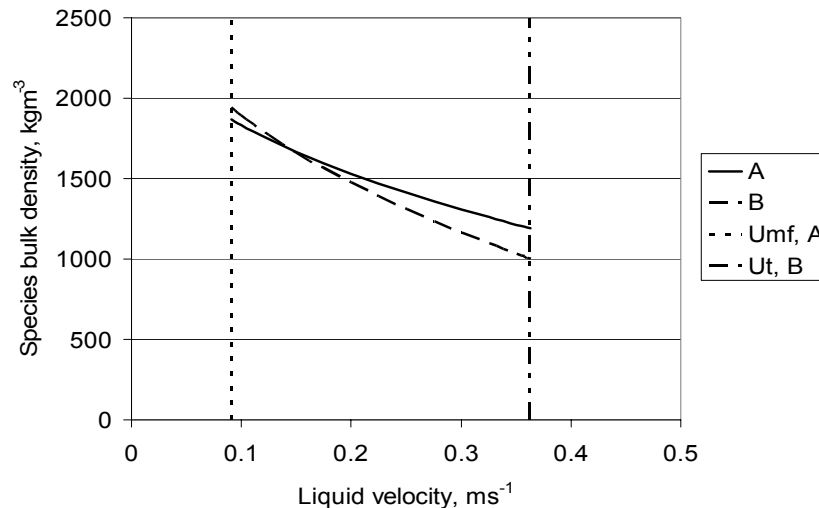

Figure 1: Theoretical plot of bulk density vs. liquid velocity for both species

Table 1: Parameters used in the CCDM simulations

Solid phase			Fluid phase	
Species	A	B	Fluid	Water
Number of particles	1000	8000	Viscosity, kgm^{-1}s^{-1}	0.001
Particle diameter, mm	5.0	2.5	Density, kgm^{-3}	1000
Particle density, kgm^{-3}	2750	3200	Bed width, m	0.15
Dry damping co'eft, kgs^{-1}	0.0181	0.0686	Bed height, m	1.30
Spring constant, Nm^{-1}	40000		Bed thickness, m	0.013
Friction coefficient	0.3		Cell height, m	0.01
Time step, µs	0.5		Cell width, m	0.01

Two completely segregated initial packings were generated as start points for the simulations: Packing 1 in which species A was at the bottom and B at the top; and Packing 2 in which species B was at the bottom of the bed with A at the top. The

fluidization of both these packings at a range of liquid velocities was then simulated. It should be noted that a "thin slice" bed geometry was used in order to reduce the overall number of particles and hence the size of the calculation – the bed thickness is small, and only interactions with the side walls were considered.

RESULTS

Figures 2a and 2b show snapshot images of the CCDM results from both initial packings, at a simulation time of around 17 seconds. It can be seen that, while the images for the simulation at U=0.14ms^{-1} are quite different, the snapshots at higher velocities have a much greater degree of similarity. This is because the systems at U=0.14ms^{-1} had not yet reached steady state, despite having been run for a relatively long time. At higher superficial fluid velocities, there is a greater driving force for segregation, and the system reaches steady conditions after a shorter time.
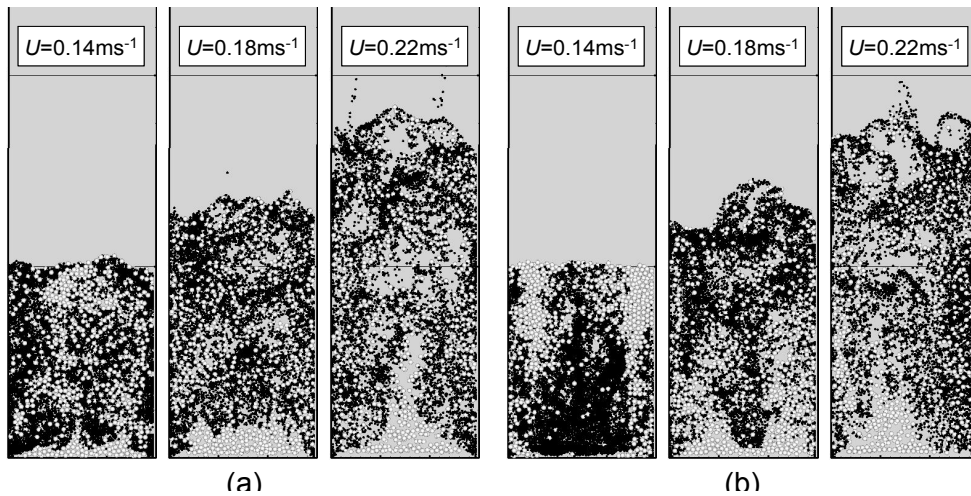

Figure 2: Snapshot images of the CCDM results at a range of superficial liquid velocities: a) starting from Packing 1; b) starting from Packing 2
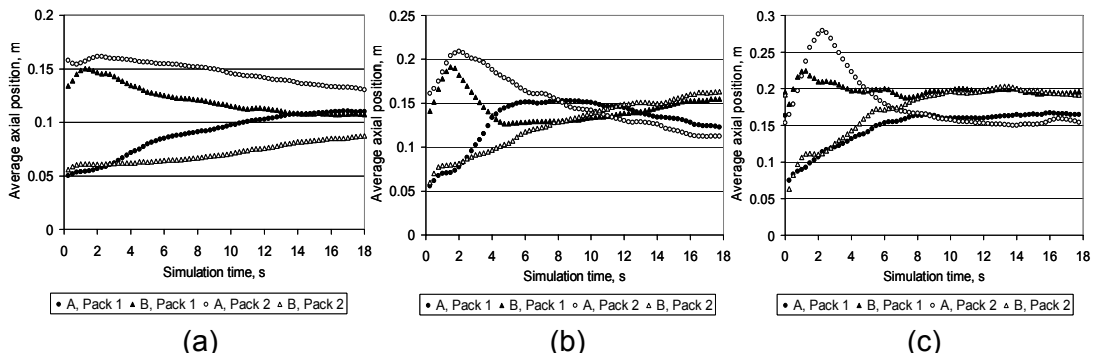

Figure 3: Plots of species' average axial positions during the simulation: a) U=0.14ms^{-1}; b) U=0.18ms^{-1}; c) U=0.22ms^{-1}

This is further demonstrated in Figures 3a-c, which show how the average axial

position of each species develops during the simulation. In Figure 3a it can be seen that the results for the two packings have not yet converged after 18 seconds of simulation time, while in Figure 3c the traces converged after around 8 seconds. The extent to which the system segregates can be seen in Figure 4, which shows how the fraction of each solid component changes as a function of height in the bed. From Figure 4c it is clear that the bed is partially segregated, with the lower part of the bed having a greater concentration of species A than of species B, whilst the upper zone of the bed contains more B than A. At lower velocities (Figures 4a and 4b) the bed is more well-mixed, suggesting that the inversion velocity is in the region of 0.14 ms^{-1}. This is broadly in agreement with the intersection of the theoretical curves shown in Figure 1. However, this result should be treated with caution since the system had not yet reached steady state.
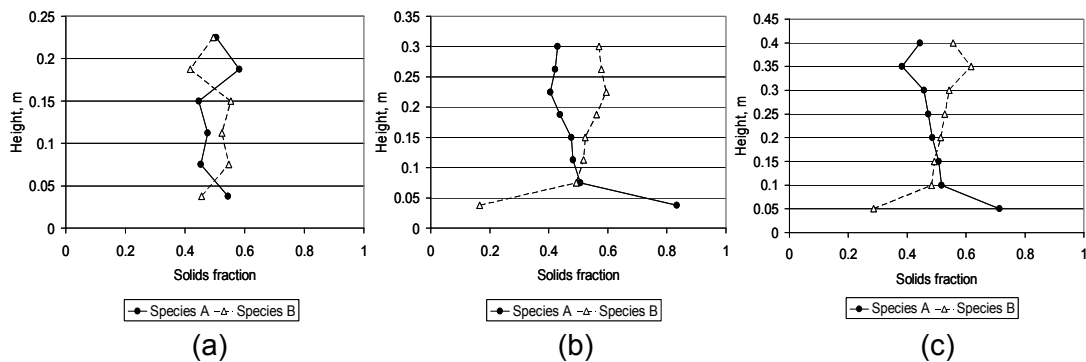

(a)   (b)   (c)

Figure 4: Variation in solids fraction with height, (results for Packing 1 only: a) *U*=0.14ms^{-1}; b) *U*=0.18ms^{-1}; c) *U*=0.22ms^{-1}

One interesting feature of the CCDM results, as shown in both Figures 2 and 3, is that the bed appears to form a relatively pure segregated layer of species A at the bottom of the bed and a mixed layer of A and B above. This is contrary to previous experimental findings (e.g. (2)), which found a tendency for the bed to form a pure layer of B at the top of the bed and either a mixed layer or a pure layer of A below, depending on the system composition. At this stage, the reason for the apparent difference between the simulation results and experiments is not altogether clear; further study is required to investigate this issue.

Figures 5a and 5b show how the bed voidage changes as a function of the superficial liquid velocity. In Figure 5a, the data from the CCDM simulations is plotted as points along with theoretical predictions of the monocomponent bed voidages at the same superficial liquid velocity (calculated using equations [5]-[8]), as well as the predictions from two literature models for the binary system voidage: the serial model (labelled SM) and the property averaging model (labeled PAM).

In the serial model (27), binary bed voidage at a given superficial liquid velocity is calculated from the theoretical values for the monocomponent beds:

$$(1-\varepsilon) = \left(0.5/1-\varepsilon_A + 0.5/1-\varepsilon_B\right)^{-1} \qquad [9]$$

In the property averaging model (13), the bed voidage is calculated with equations

[5]-[8], but with averaged properties for the two species:

$$d_p = \left(0.5 / d_{pA} + 0.5 / d_{pB}\right)^{-1} \quad : \quad \rho_p = 0.5 \rho_{pA} + 0.5 \rho_{pB} \qquad [10]$$

In Figure 5b, the same CCDM points for the binary bed are plotted along with curves obtained from CCDM simulations of the two monocomponent systems, and the serial model prediction using the data from the CCDM monocomponent systems.
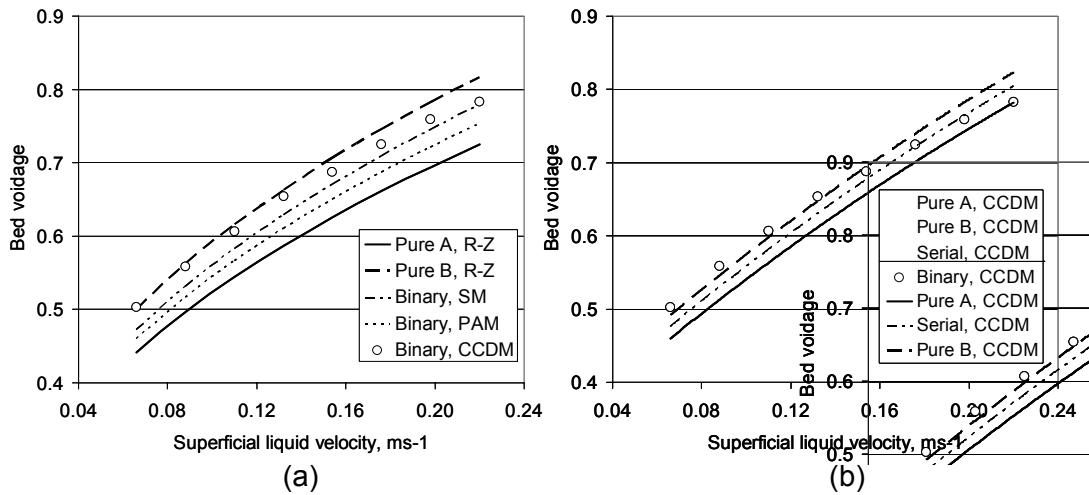

Figure 5: Comparison of simulation results with model predictions: a) Bed voidage; b) Bulk density, as a function of superficial liquid velocity

It can be seen in Figures 5a and 5b that the CCDM results agree reasonably well with the SM predictions using both the theoretical (5a) and CCDM monocomponent data (5b), although there is some deviation from the curves at lower liquid velocities, with the binary CCDM datapoints being higher than the model predictions. In fact, in Figure 5b, some of the lower datapoints lie outside the region enclosed by the monocomponent curves. At this stage, the reason for this deviation is not clear. It may be that the system geometry (i.e. a "thin slice" bed) has an effect on the system voidage. Further work is necessary to determine if this is in fact the case.

CONCLUSIONS

Preliminary CCDM simulations of a binary-solid fluidized bed have shown that the degree of segregation in the system changes with liquid velocity, although at low velocities steady state was not reached in the simulation time. Further work is needed to explain both the deviation in the simulated bed voidages from literature model predictions, and the reason why the segregation patterns in the simulations differ from those found in previous experimental studies.

ACKNOWLEDGEMENTS

REFERENCES

1   Escudie, R., Epstein, N., Grace, J.R., & Bi, H.T., (2006). Chemical Engineering Science, 61(5): 1528-39.
2   Moritomi, H., Iwase, T., & Chiba, T., (1982). Chemical Engineering Science, 37(12): 1751-7.
3   Di Felice, R., Gibilaro, L.G., Waldram, S.P., & Foscolo, P.U., (1987). Chemical Engineering Science, 42(4): 639-52.
4   Moritomi, H., Yamagishi, T., & Chiba, T., (1986). Chemical Engineering Science, 41(2): 297-305.
5   Epstein, N. & LeClair, B.P., (1985). Chemical Engineering Science, 40(8): 1517-26.
6   Asif, M., (2004). Powder Technology, 145(2): 113-22.
7   Funamizu, N. & Takakuwa, T., (1995). Chemical Engineering Science, 50(19): 3025-32.
8   Jean, R.-H. & Fan, L.-S., (1986). Chemical Engineering Science, 41(11): 2811-21.
9   Gibilaro, L.G., Di Felice, R., Waldram, S.P., & Foscolo, P.U., (1986). Chemical Engineering Science, 41(2): 379-87.
10 Rasul, Mohammad G., (2003). Particle & Particle Systems Characterization, 20(6): 398-407.
11 Asif, M., (2002). Powder Technology, 127(3): 226-38.
12 Hu, X., (2002). Chemical Engineering Science, 57(15): 3149-53.
13 Asif, M., (1998). Chemical Engineering & Technology, 21(1): 77-82.
14 Howley, M.A. & Glasser, B.J., (2002). Chemical Engineering Science, 57(19): 4209-26.
15 Syamlal, M. & O'Brien, T.J., (1988). International Journal of Multiphase Flow, 14(4): 473-81.
16 Escudie, R., Epstein, N., Grace, J.R., & Bi, H.T., (2006). Chemical Engineering Science, 61(20): 6667-90.
17 Cundall, P.A. & Strack, O.D.L., (1979). Geotechnique, 29(1): 47-65.
18 Anderson, T.B. & Jackson, R., (1967). Industrial and Engineering Chemistry Fundamentals, 6(4): 527-39.
19 Patankar, S.V., (1980). Numerical heat transfer and fluid flow. Hemisphere, London.
20 Xu, B.H. & Yu, A.B., (1997). Chemical Engineering Science, 52(16): 2785-809.
21 Di Felice, R., (1994). International Journal of Multiphase Flow, 20(1): 153-9.
22 Tsuji, Y., Morikawa, Y., & Mizuno, O., (1985). Journal of Fluids Engineering-Transactions of the Asme, 107(4): 484-8.
23 Fan, L.S. & Zhu, C., (1998). Principles of gas-solid flows. Cambridge University Press, Cambridge; New York.
24 Joseph, G.G., Zenit, R., Hunt, M.L., & Rosenwinkel, A.M., (2001). Journal of Fluid Mechanics, 433: 329-46.
25 Richardson, J.F. & Zaki, W.N., (1954). Transactions of the Institution of Chemical Engineers, 32: 35-53.
26 Coulson, J.M., Richardson, J.F., Backhurst, J.R., & Harker, J.H., (1991). Chemical engineering. Vol.2, particle technology and separation processes. 4th ed. Butterworth-Heinemann, Oxford.
27 Epstein, N., Leclair, B.P., & Pruden, B.B., (1981). Chemical Engineering Science, 36(11): 1803-9.